Whole-brain functional imaging with two-photon light-sheet microscopy

To the Editor: Several studies recently demonstrated that one-photon (1P) light-sheet imaging gives access to the spontaneous activity of a large fraction of the zebrafish larval brain at nearly single-cell resolution[1–3]. This imaging method, however, requires an intense and extended illumination at a wavelength ($\lambda = 488$ nm) that lies within the most sensitive region of the fish visible spectrum[4] and therefore likely stimulates the blue photoreceptors in the retina as well as other photosensitive cells[5]. As an alternative, we report on brain-wide three-dimensional (3D) neural recordings during visuomotor integration in zebrafish larvae using two-photon (2P) light-sheet imaging[6] at a wavelength of 930 nm combined with visual stimulation.

The extent to which 1P illumination interferes with visually driven processes is critical as it determines the suitability of light-sheet imaging for behavioral neuroscience. Vladimirov *et al.* recently showed that the optomotor reflex and the associated motor-adaptation behavior could be normally evoked during 1P light-sheet imaging[3]. However, these robust behaviors are not driven by the blue and UV cones[7] and are not even affected by ablation of the optic tectum, the largest visual center in fish[8]. To evaluate the relevance of 2P excitation for whole-brain visual studies and directly compare 1P and 2P excitation regimes, we implemented a twin light-sheet system (**Fig. 1a**, **Supplementary Figs. 1** and **2**, and **Supplementary Table 1**). This system provided similar axial and lateral resolutions in the 1P and 2P configurations and enabled functional imaging with cellular resolution in ~80% of the brain volume (**Supplementary Figs. 3** and **4**), without measurable photobleaching during long-term (1-h) recordings. We exposed 4- to-6-d-old zebrafish larvae expressing the calcium indicator GCaMP5G to a series of blue flashes of increasing intensity. We successively recorded evoked neural activity at 4 Hz using 1P and 2P imaging in approximately the same layer of the

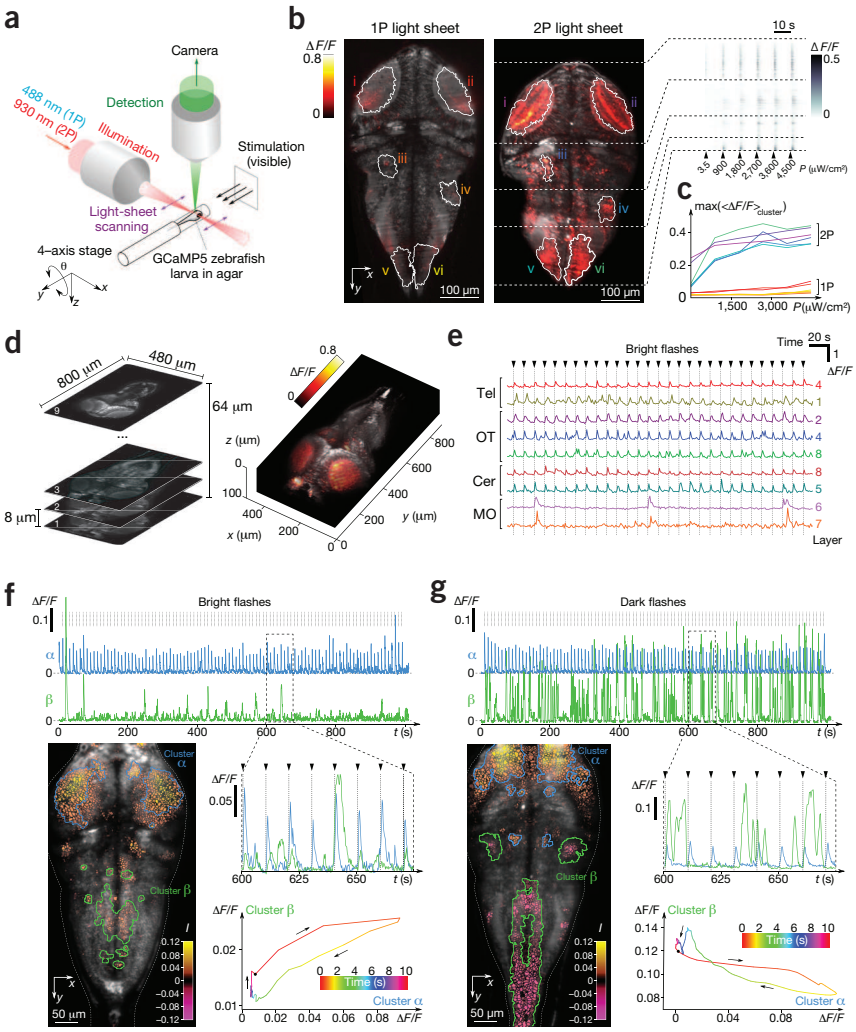

Figure 1 | Two-photon (2P) light-sheet functional imaging of visually evoked neural activity. (**a**) The 1P/2P light-sheet imaging system. (**b**) Left, brain-wide section of a 5-d-old larva overlaid with the flash-evoked neural response ($\Delta F/F$, 250 ms after the flash) measured with 1P and 2P light-sheet imaging. Images were recorded at 4 Hz and averaged over 20 successive flash presentations at 4,500 µW cm^{-2}. Right, post-stimulus raster plot of 3,283 neurons and neuropil regions. Data are averaged over 20 flash presentations for each stimulus intensity. (**c**) Post-stimulus response of the regions contoured in **b** for various stimulus intensities. Data in **b**,**c** are representative of $n = 9$ larvae. (**d**) 3D recording of activity evoked by 3,600 µW cm^{-2} flashes. A stack of nine layers with 8-µm intervals was recorded every second, yielding a total of 36,063 neurons monitored at 1 Hz. The 3D volume rendering of the fish brain shows the $\Delta F/F$ response measured immediately after the flash. (**e**) Typical signals of flash-responsive neurons in different brain regions (Tel, telencephalon; OT, optic tectum; Cer, cerebellum; MO, medulla oblongata). (**f**,**g**) Network analysis of flash-induced neural responses. The images display the stimulus-averaged response to a 200-ms-long bright flash (**f**) or a 1-s-long dark flash (**g**). The color code in the micrographs represents the variation of $\Delta F/F$ averaged over the first 1.5 s after the flash. The blue and green lines delimit the two most prominent neuronal clusters responding to bright and dark red flashes as computed using the k-means algorithm ($k = 12$), whose time dynamics are shown in the three associated graphs. For bright flashes, the activity of the hindbrain cluster was enhanced after the flash onset, whereas dark flashes induced a transient reduction of its activity.

same fish. The imaged section was chosen so as to avoid direct exposure of the eyes to the illumination beam. During 2P imaging, the flashes elicited acute neural responses in various regions of the brain (**Fig. 1b** and **Supplementary Video 1**) even at the lowest flash intensity (3.5 μW cm^{-2}). At an illumination intensity compatible with 3D imaging, the response during 1P imaging was either abolished or greatly attenuated (**Fig. 1b** and **Supplementary Video 2**). To quantify this observation, we extracted the maximum of the post-stimulus signal in the five most responsive regions in both experiments. In 2P imaging, all regions displayed a substantial response at the lowest stimulus intensity, which rapidly reached a plateau as the visual stimulation became more intense (**Supplementary Figs. 5** and **6,** and **Fig. 1c**). During 1P imaging, the visually evoked activity was mostly confined to the tectal neuropil, the region that receives direct projections from retinal ganglion cells. To elicit measurable signals in other brain areas, the stimulus intensity had to be increased up to 4,500 μW cm^{-2}, beyond physiologically relevant levels.

The exact mechanism by which 1P illumination leads to the observed reduction in visual sensitivity remains to be elucidated. The photoreceptors in the retina may receive excitation light scattered by the observation chamber or by the brain tissue, increasing the response threshold to subsequent visual stimuli. Alternatively, the visually evoked neural response may be attenuated owing to direct activation of light-sensitive cells throughout the brain. In any case, our results highlight the potential problems associated with visible illumination wavelengths and argue for the use of near-infrared wavelengths when studying visually driven processes.

2P light-sheet imaging combines the advantages of near-infrared illumination with the high speed of light-sheet microscopy. We produced 3D maps of flash-responsive neurons in a single experiment by sequentially moving the recorded plane across the brain and simultaneously recorded >36,000 individual neurons at 1 Hz (**Fig. 1d**,**e**, **Supplementary Fig. 7** and **Supplementary Video 3**), without compromising signal-to-noise ratio. Brain-wide parallel recording of multiple brain regions opens the possibility of identifying extended clusters of neurons by analyzing the structure of the correlation matrix (**Supplementary Methods** and **Supplementary Fig. 8**). Cluster dynamics can then provide a low-dimensional description of the post-stimulus time sequence of brain activity (**Fig. 1f**,**g** and **Supplementary Fig. 9**).

In conclusion, we demonstrated that near-infrared 2P light-sheet imaging is suitable for 3D brain-wide functional imaging in zebrafish larvae at cellular resolution. Notably, this imaging method eliminates the photostimulation associated with 1P functional imaging. Although the latter does not abolish robust visuomotor reflexes, we showed that it compromises visual perception in the blue domain. Therefore, 2P light-sheet imaging is a suitable alternative method for whole-brain network analysis of neural processes that require fine control over the visual stimuli or that are sensitive to the photic environment.

Note: Any Supplementary Information and Source Data files are available in the online version of the paper (doi:10.1038/nmeth.3371).

ACKNOWLEDGMENTS
We thank F. Engert (Harvard University) for providing the Huc:GCaMP5G strain. The study was partly supported by Agence Nationale de la Recherche (contracts ANR-2010-JCJC-1510-01, ANR-11-EQPX-0029, ANR-10-INBS-04), Fondation Louis D. de l'Institut de France, European Union Seventh Framework Program (Marie Curie International Reintegration Grant no. 268379).

COMPETING FINANCIAL INTERESTS
The authors declare no competing financial interests.

Sébastien Wolf[1,2], Willy Supatto[3], Georges Debrégeas[1,2], Pierre Mahou[3], Sergei G Kruglik[1,2], Jean-Marc Sintes[3], Emmanuel Beaurepaire[3] & Raphaël Candelier[1,2]

[1]Sorbonne Universités, Université Pierre et Marie Curie Paris 06, Paris, France. [2]Centre National de la Recherche Scientifique (Unité Mixte de Recherche 8237), Laboratoire Jean Perrin, Paris, France. [3]Laboratoire Optique et Biosciences, Ecole Polytechnique, Centre National de la Recherche Scientifique (Unité Mixte de Recherche 7645) et Institut National de la Santé et de la Recherche Médicale (U1182), Palaiseau, France.
e-mail: georges.debregeas@upmc.fr or raphael.candelier@upmc.fr

1. Panier, T. *et al. Front. Neural Circuits* **7**, 65 (2013).
2. Ahrens, M.B., Orger, M.B., Robson, D.N., Li, J.M. & Keller, P.J. *Nat. Methods* **10**, 413–420 (2013).
3. Vladimirov, N. *et al. Nat. Methods* **11**, 883–884 (2014).
4. Risner, M.L., Lemerise, E., Vukmanic, E.V. & Moore, A. *Vision Res.* **46**, 2625–2635 (2006).
5. Fernandes, A.M. *et al. Curr. Biol.* **22**, 2042–2047 (2012).
6. Truong, T.V., Supatto, W., Koos, D.S., Choi, J.M. & Fraser, S.E. *Nat. Methods* **8**, 757–760 (2011).
7. Portugues, R. & Engert, F. *Curr. Opin. Neurobiol.* **19**, 644–647 (2009).
8. Roeser, T. & Baier, H. *J. Neurosci.* **23**, 3726–3734 (2003).

MiXCR: software for comprehensive adaptive immunity profiling

To the Editor: High-throughput sequencing is gaining importance in adaptive immunity studies, demanding efficient software solutions for immunoglobulin (IG) and T-cell receptor profiling[1]. Here we report MiXCR (available at http://mixcr.milaboratory.com/ and https://github.com/milaboratory/mixcr/), a universal framework that processes big immunome data from raw sequences to quantitated clonotypes. MiXCR efficiently handles paired- and single-end reads, considers sequence quality, corrects PCR errors and identifies germline hypermutations. The software supports both partial- and full-length profiling and employs all available RNA or DNA information, including sequences upstream of V and downstream of J gene segments (**Fig. 1**, **Supplementary Note 1** and **Supplementary Table 1**).

In contrast with previous software[2–5], MiXCR employs an advanced alignment algorithm that processes tens of millions of reads within minutes, with accurate alignment of gene segments even in a severely hypermutated context (**Supplementary Note 2** and **Supplementary Tables 2–6**). In paired-end sequencing analysis, MiXCR aligns both reads and aggregates information from both alignments to achieve high V and J gene assignment accuracy. It handles mismatches and indels and thus is suitable even for sequences with many errors and hypermutations. MiXCR employs a built-in library of reference germline V, D, J and C gene sequences for human and mouse based on corresponding loci from GenBank[6].

MiXCR further assembles identical and homologous reads into clonotypes, correcting for PCR and sequencing errors using a heuristic multilayer clustering. Additionally, it rescues low-quality reads by mapping them to previously assembled high-quality clonotypes[7] to preserve maximal quantitative information (**Supplementary Note 3**). The Illumina MiSeq platform currently allows for deep full-length IG repertoire profiling with ~20 million long paired-end reads. MiXCR captures all complementarity-determining regions (CDRs) and framework regions of immune genes and permits the assembly of full-length clonotypes. Flexibility to analyze partial-length data is also provided, allowing, for example, users to group reads into clonotypes

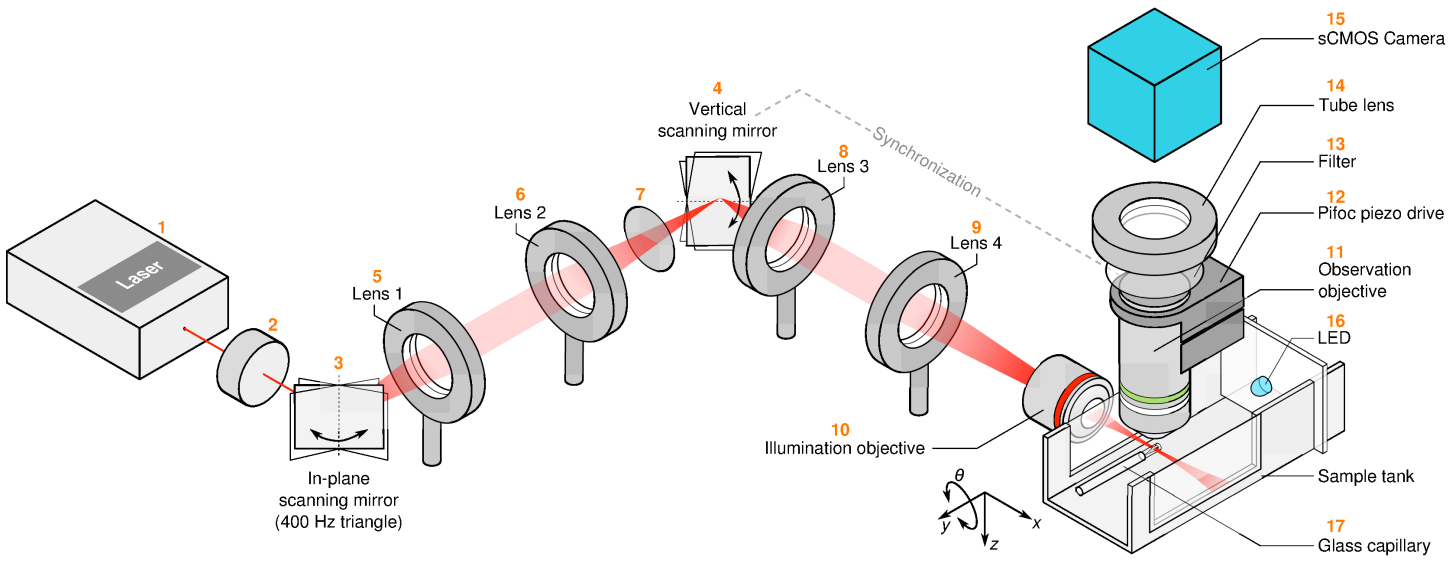

Supplementary Figure 1

Scheme of the 1P/2P light-sheet microscopy setups.

The optical components are listed in **Supplementary Table 1**.

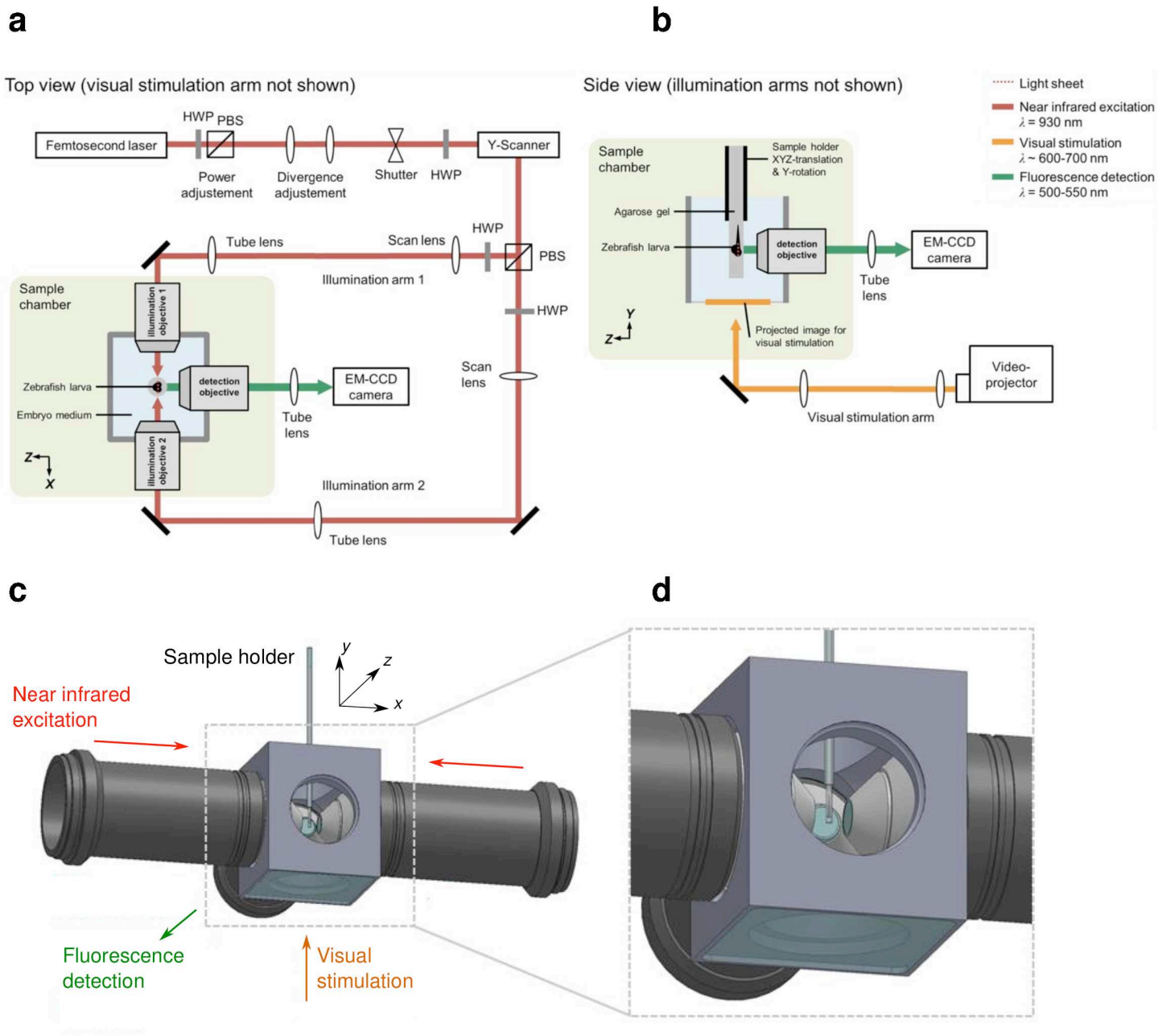

Supplementary Figure 2

Two-photon light-sheet microscope with visual stimulation.

(**a,b**) Scheme of the two-photon light-sheet microscope with visual stimulation used to perform cluster analysis of dark- and bright-flash induced responses. HWP: half wave plate; PBS: polarization beam splitter; EMCCD: electron-multiplying charge-coupled device camera. (**c**) 3D-rendering of the liquid-filled specimen chamber with objective lenses on the lateral sides, sample held from the top and transparent screen for visual stimulation at the bottom. (**d**) Blow-up of the specimen chamber.

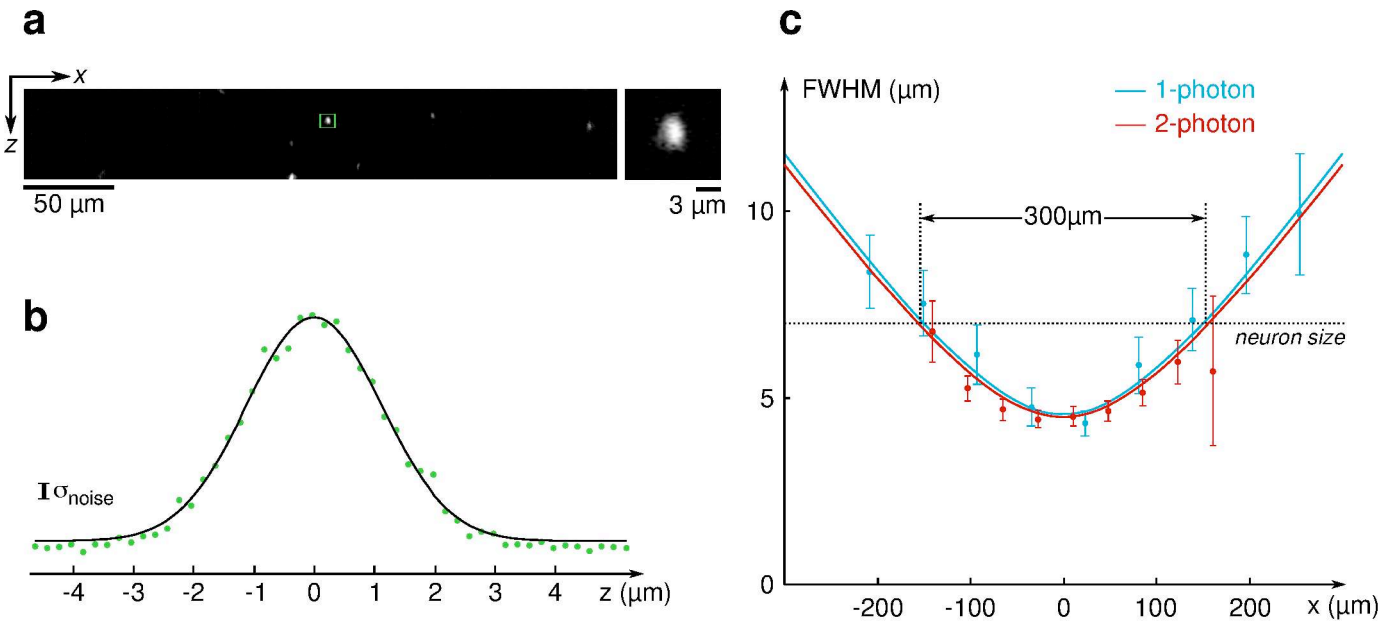

Supplementary Figure 3

Axial resolution.

(**a**) Vertical cross-section of an agarose gel cylinder containing 100 nm in diameter fluorescent beads. The image was reconstructed from a series of horizontal sections, separated by 0.2 µm intervals, imaged using the 2P light-sheet setup. (**b**) Axial profile of the fluorescence intensity of the bead identified in (a) by the green rectangle. The solid line shows the best gaussian fit to the profile. (**c**) Full width at half maximum (*FWHM*) of the measured fluorescence profile, for 1P and 2P light-sheet imaging, as a function of the bead position along the illumination axis. The profiles are fitted with equations (1) and (2). The FWHM in the region delimited by the two vertical lines falls below the typical inter-soma distance in zebrafish larvae (≈6.5 µm). In this region, the optical sectioning is thus compatible with single-cell resolution.

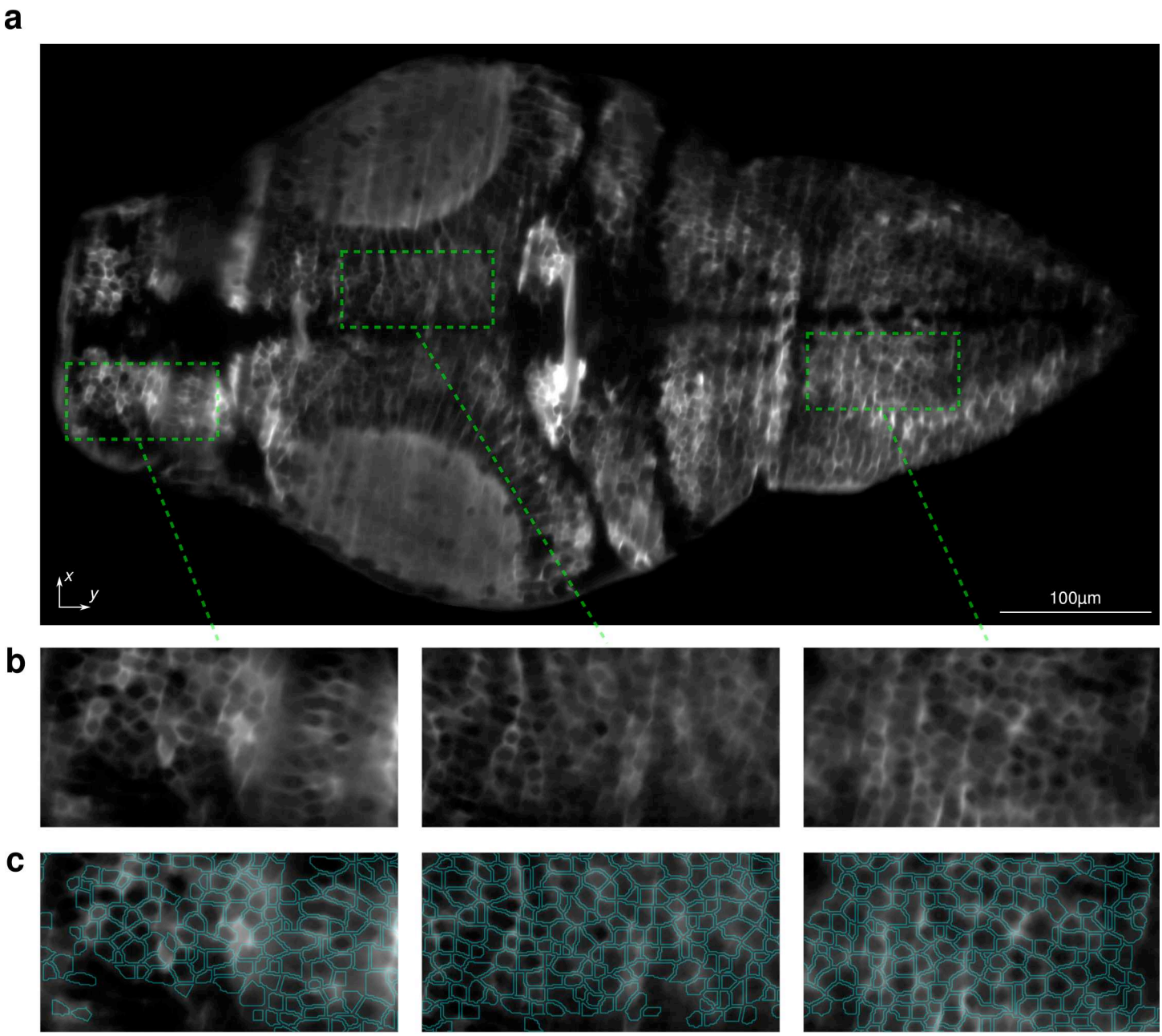

Supplementary Figure 4

Automatic image segmentation.

(**a**) Charactersitic brain-wide section of the larva's brain obtained using 2P light-sheet imaging. (**b**) Blowups of different regions. From left to right: telencephalon, optic tectum, hindbrain. (**c**) Result of the automatic segmentation procedure leading to the identification of ROIs associated with individual somas.

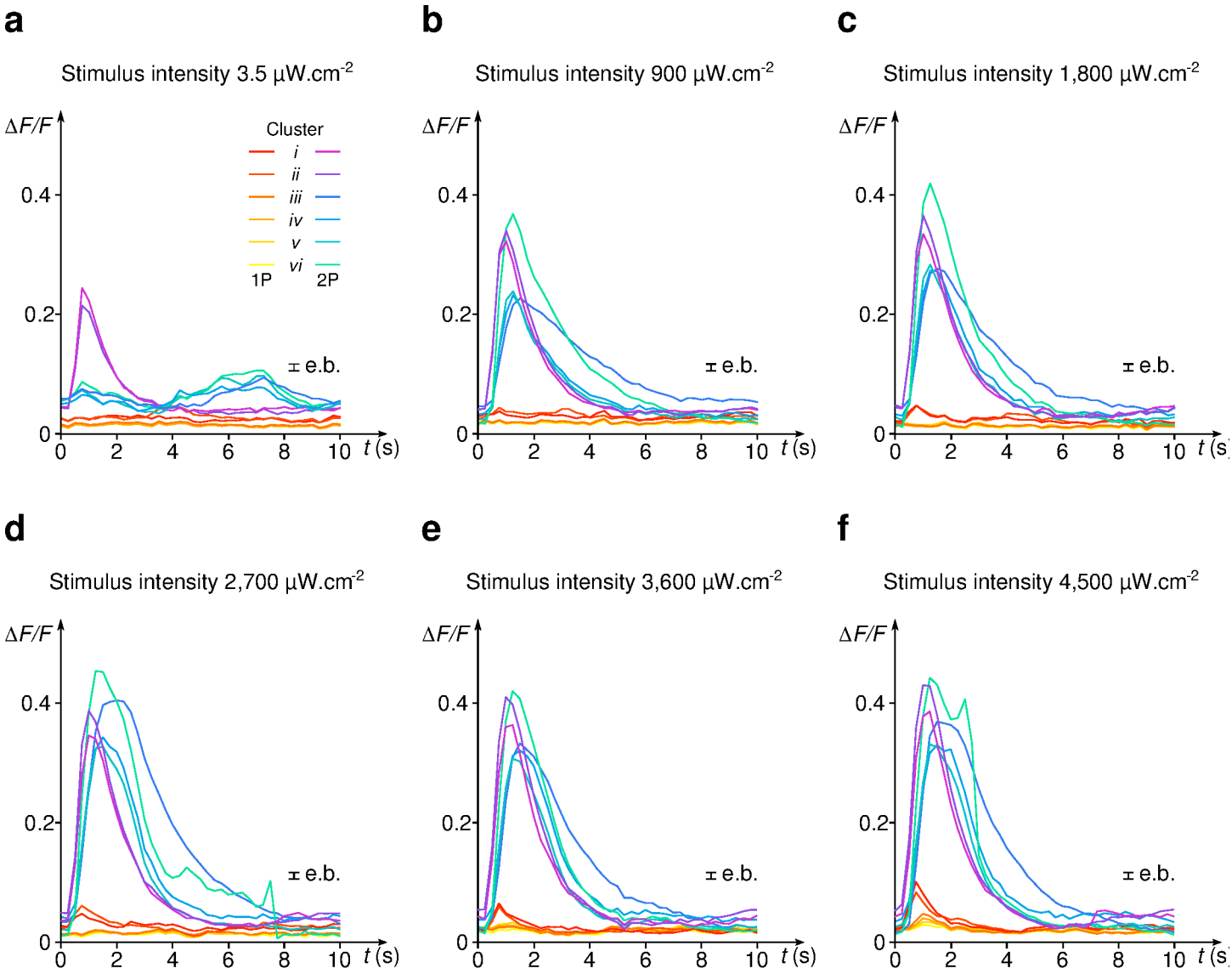

Supplementary Figure 5

Comparison between flash-evoked response under 1P *vs* 2P imaging (1P illumination power, 500 µW).

(**a-e**) Post-stimulus response averaged over the 5 most responsive subregions contoured in **Fig. 1**, for 6 increasing stimulus intensity. The graphs show that for all tested stimulus intensities, the response is either abolished or greatly reduced in 1P imaging, with respect to 2P imaging.

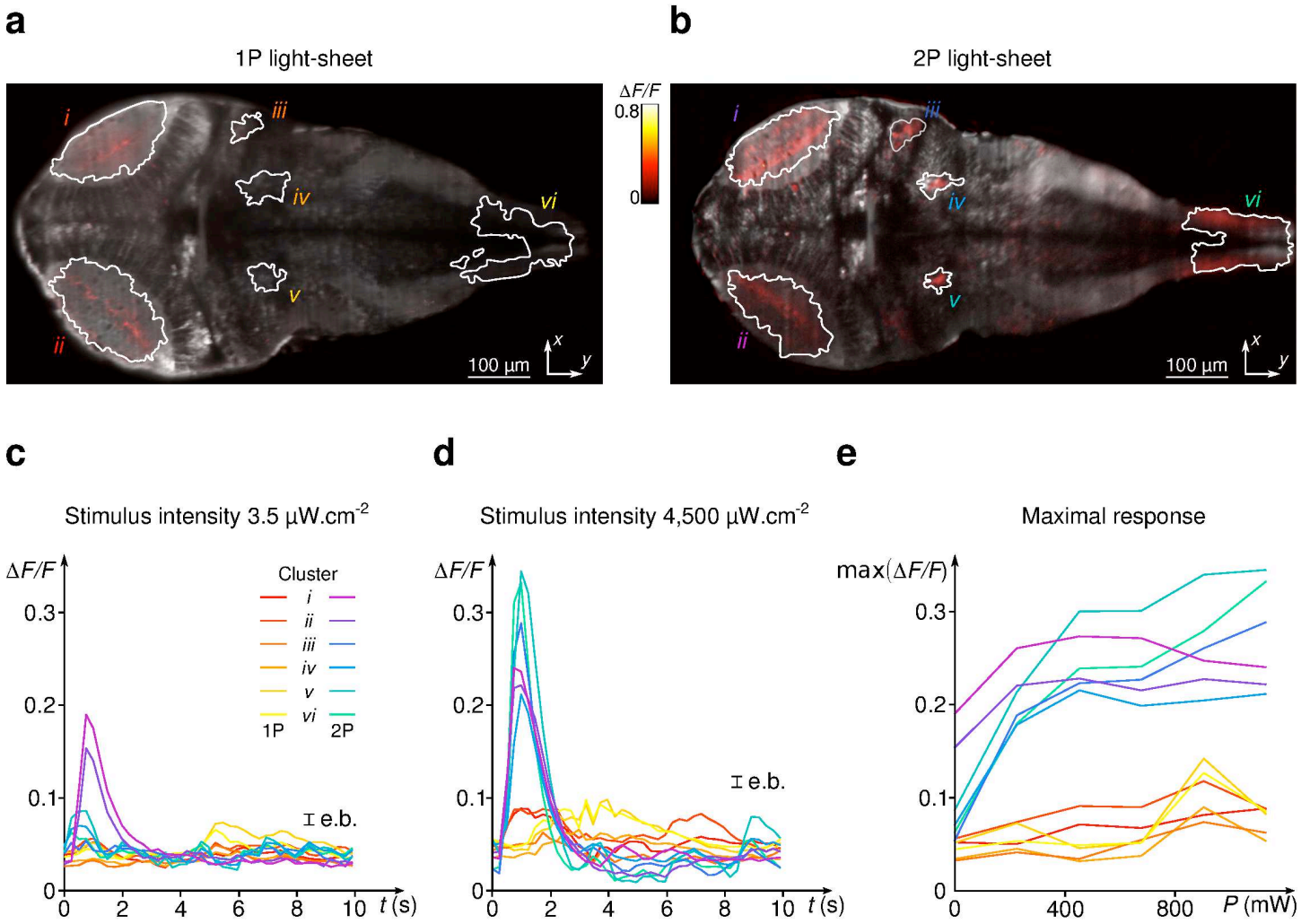

Supplementary Figure 6

Comparison between flash-evoked response under 1P *vs* 2P imaging at low 1P illumination power (100 µW).

(**a-b**) Stimulus-averaged response, measured 250 ms after the flash in 1P and 2P imaging, respectively (*ΔF/F* in color code). (**c-d**) Post-stimulus response averaged over the 5 subpopulations contoured in (a-b) (most responsive regions), for the lowest (c) and highest (d) stimulus intensity. (**e**) Evolution of the maximum response for each contoured region as a function of the stimulus intensity. Even at this low illumination power, 1P light-sheet imaging still induces a severe reduction of visual sensitivity.

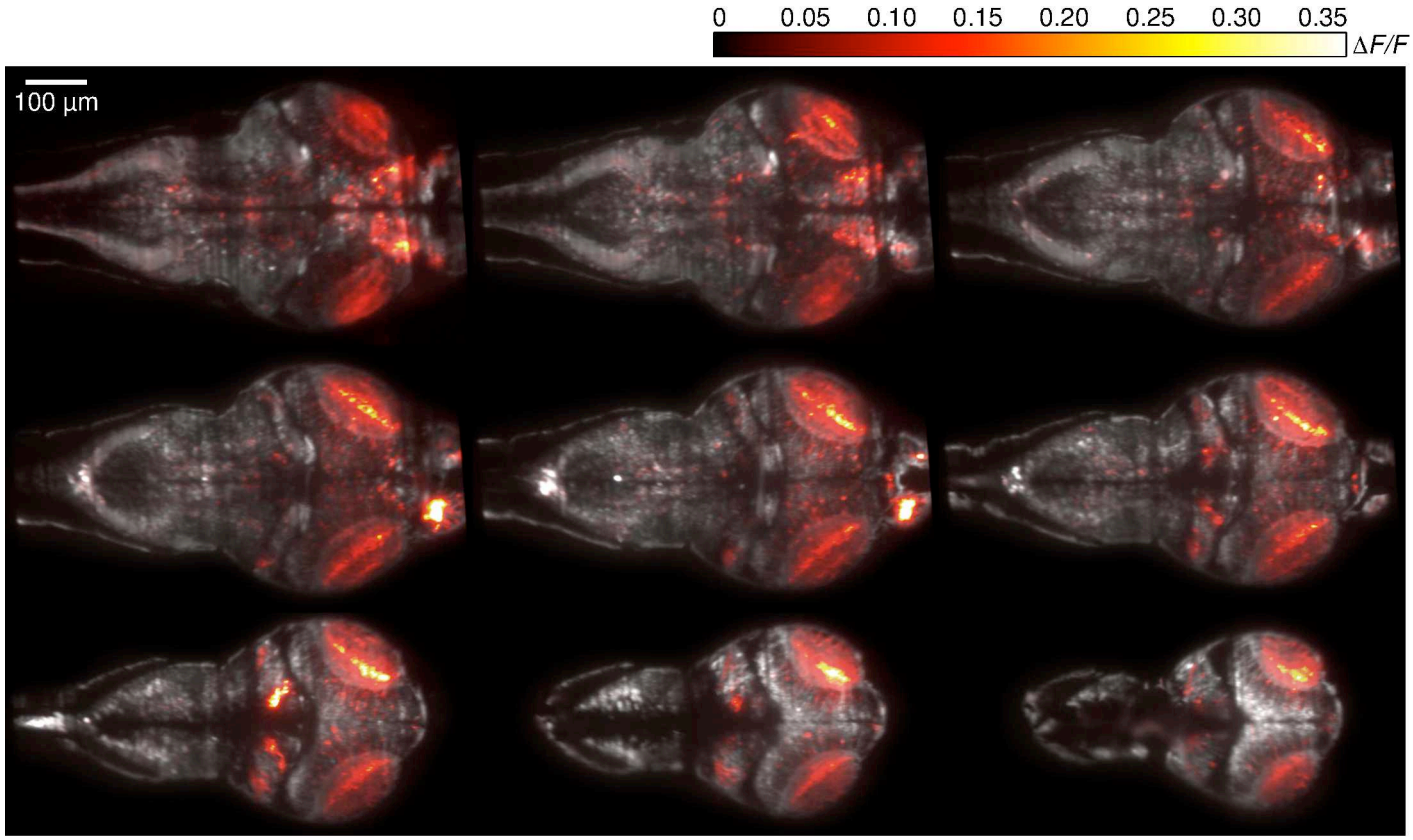

Supplementary Figure 7

3D imaging.

Nine layers were acquired at 1 Hz across a 5 day old larva brain (90 ms exposure per layer). On the sections shown, the average neural response (*ΔF/F*), measured in the first second following a 3,600 µW.cm^{-2} flash, is color coded (120 flashes, 10 s intervals between flashes).

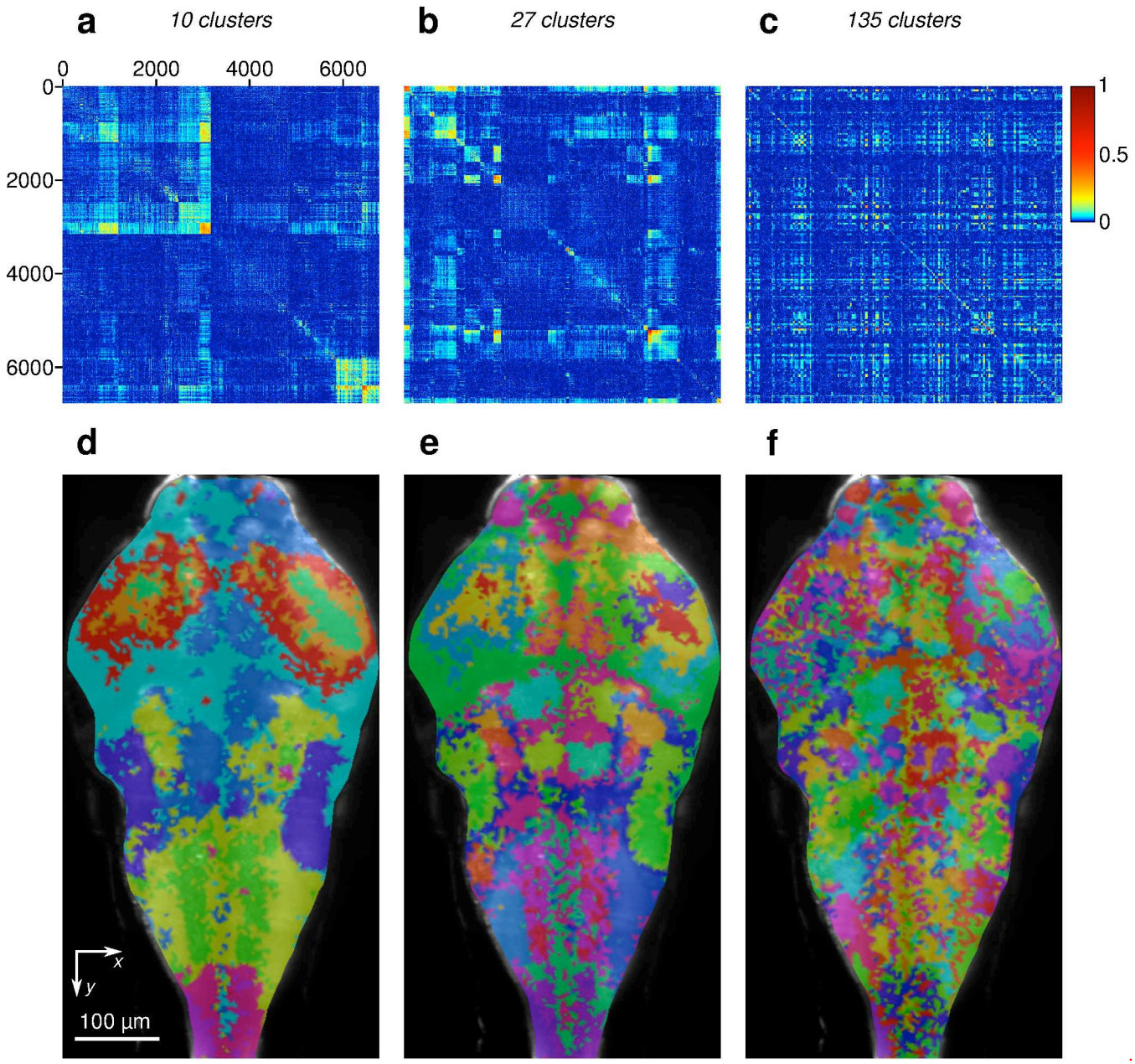

Supplementary Figure 8

Cluster analysis performed on a 1,050 s-long, 100 bright flashes recording.

(**a-c**) The k-means algorithm is computed for different k-values on the Pearson matrix that conveys neuron-neuron correlations. The clusters appear as square blocks in the re-ordered Pearson matrix. (**d-f**) The spatial structure of the different clusters is shown: each color corresponds to one cluster. These maps reveal the functional organization of the brain at different scales.

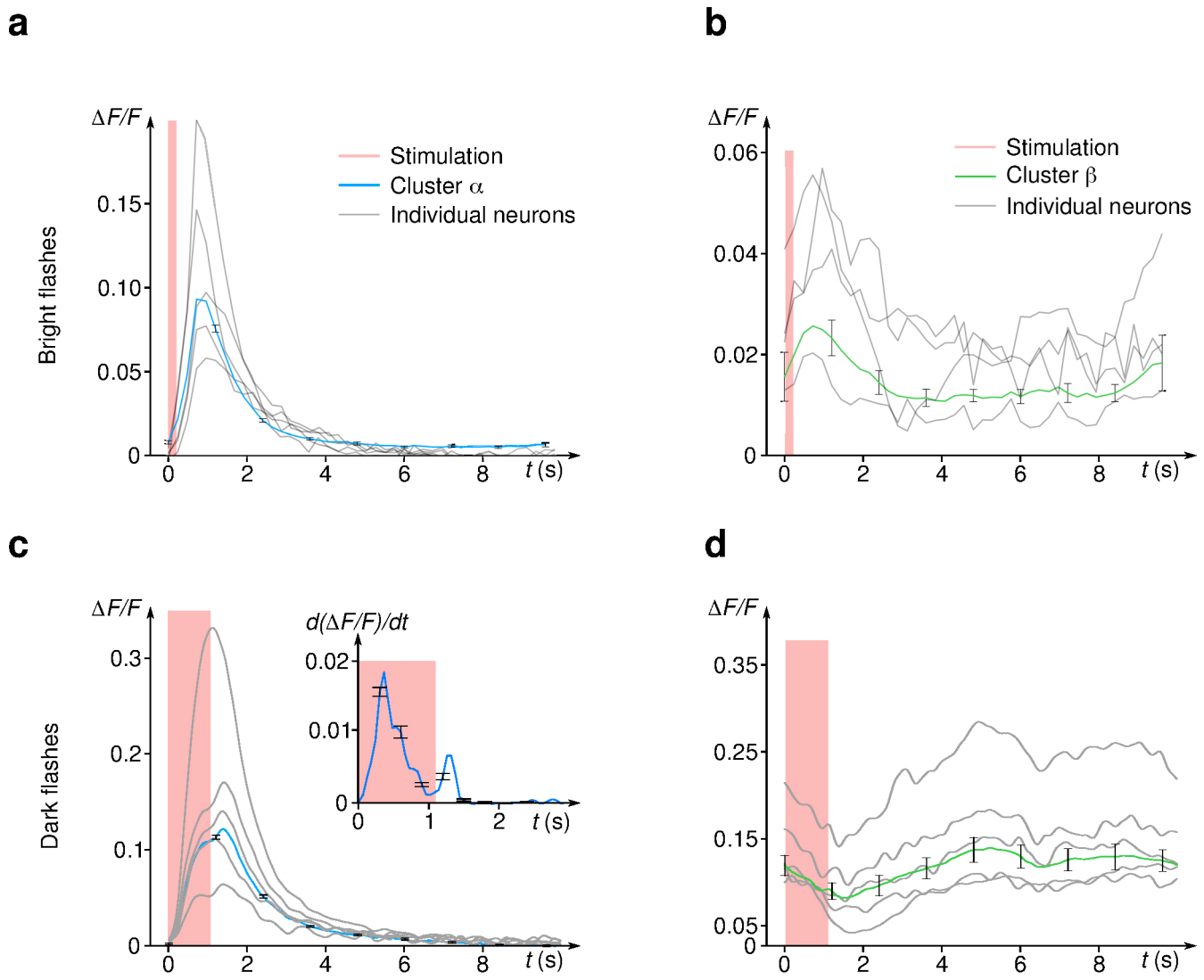

Supplementary Figure 9

Bright *vs* dark flash-induced response.

Using the k-means algorithm (k = 12), we identified the two most prominent neuronal clusters whose topography is shown in **Fig. 1g-h**. Across-stimuli responses of the (a) visual α and (b) hindbrain β clusters for 200 ms-long bright flashes. The blue curve is the cluster-averaged response. Characteristic traces of individual neurons from the clusters are shown in grey. (**c-d**) Similar analysis performed for 1 s-long dark flashes on a different larva. The inset in (c) reveals that the visual cluster shows a positive transient response to both the onset and offset of the stimulus. In all graphs, the red rectangle indicates the stimulation period.

Supplementary tables

	Part	1P light-sheet mircoscope	2P light-sheet mircoscope
1	Laser	488 sapphire, Coherent	Mai Tai, Spectra-Physics
2	Precompensator	-	Deep See
3	Galvanometer mirror (xy)	8315K, Cambridge Technology	8315K, Cambridge Technology
4	Galvanometer mirror (xz)	8315K, Cambridge Technology	8315K, Cambridge Technology
5	Scanning lens (Lens 1)	$F = 50$	$F = 50$
6	Tube lens (Lens 2)	$F = 150$	$F = 150$
7	Polarization beam splitter	-	CM1-PBS252, ThorLabs
8	Scanning lens (Lens 3)	$F = 100$	$F = 150$
9	Tube lens (Lens 4)	$F = 200$	$F = 300$
10	Illumination Objective	Zeiss EC Plan-Neofluar 5x	IR 5x Olympus LMPLS5xIR
11	Observation Objective	20x Olympus XLUMPlanFLN	20x Olympus XLUMPLFLN
12	Objective piezo drive	Mipos 500 SG,Triptics	Mipos 500 SG,Triptics
13	Emission filter	Notch-filter, 488 nm	Low-pass filter (cut-off 800 nm)
14	Camera tube lens	$F = 150$	$F = 150$
15	sCMOS camera	PCO.edge 5.5	PCO.edge 4.2
16	LED	470 nm, 5 cd, 15° aperture	470 nm, 5 cd, 15° aperture
17	Capillary	Internal diameter 1 mm	Internal diameter 1 mm

Supplementary table 1 | Main components of the 1P and 2P twin ligh-sheet microscopes.

Supplementary Methods

Larvae preparation

The experiments were performed on zebrafish *nacre* mutant expressing the calcium indicator GCaMP5G[9] under the control of the pan-neuronal promoter *elavl3*. The embryos were collected and raised at 28.5°C in E3 embryo medium, and kept under 14/10h on/off light cycles. Larvae aged 4–6d.p.f. were mounted in a 1 mm in diameter cylinder of low-melting point agarose (1.8% in concentration)[1]. To prevent movements of the animal during functional imaging, the agarose contained a paralyzing agent (Pancuronium bromide, 0.3 mg/mL). All experiments were approved by *Le Comité d'Ethique pour l'Expérimentation Animale Charles Darwin*.

Optical setup for 1P/2P comparison

In order to compare visual responses during 1P and 2P imaging, we built a twin light-sheet microscope (**Supplementary Fig. 1** and **Supplementary Table 1**), with similar optical configurations, using the same specimen chamber and visual stimulation device.

Two-photon light-sheet microscopy. A titanium:sapphire laser (Mai Tai, Spectra-Physics) was used to deliver a near infrared pulsed excitation at the sample with 100-200 fs pulse duration, 80 MHz repetition rate and λ = 930 nm central wavelength. The excitation power at the sample was adjusted using a half wave plate and a polarization beam splitter (CM1-PBS252, Thorlabs) to 280 mW (measured before the illumination objective). This power allowed for a contrast and a signal-to-noise ratio close to what we obtain with the 1P setup at similar exposure time, and was low enough to avoid damage in brain tissues. The light-sheet microscope included two galvanometer mirrors (6215H/8315K, Cambridge Technology), associated with two pairs of scan and tube lenses, and a low NA illumination objective (5 x 0.1NA, LMPLNXIR, Olympus). The weakly focused laser beam was scanned at 400 Hz over 800 µm in the Y-direction by the galvanometer mirror, creating an illumination light-sheet in the XY-plane.

The detection arm consisted of a water-immersion objective (20 x 1.0NA, XLUM-PLFLN, Olympus) mounted vertically onto a piezo nanopositioner (Piezosystem Jena MIPOS 500), allowing precise adjustment of the focus plane with the light sheet. The fluorescence light was collected by a tube lens (150 mm focal length, Thorlabs AC254-150-A) and passed through a low-pass filter (NF488-15, Thorlabs) to eliminate 930 nm photons. The image was then formed onto a sCMOS sensor (PCO.edge 4.2, PCO). The 20x magnification yielded a field of view of 0.8 x 0.8 mm^2, with a pixel area of 0.4 x 0.4 μm^2. The 3D recordings were performed at a rate of 10 frames per second.

One-photon light-sheet microscopy. The one-photon light-sheet microscope was a modified version of a system described earlier[1]. It used a 488 nm solid-state diode laser (488 Sapphire, Coherent) at a power of 500 µW (measured before the illumination objective), two galvanometer mirrors (6215H/8315K, Cambridge Technology), associated with two pairs of scan and tube lenses, and a low NA illumination objective (5 x 0.16 NA, Zeiss EC Plan-Neofluar).

The detection arm consisted of a water-immersion objective (20 x 0.95 NA, XLUMPlanFL, Olympus) mounted vertically onto a piezo nanopositioner (Piezosystem Jena MIPOS 500). The fluorescence light was collected by a tube lens (150 mm focal length, Thorlabs AC254-150-A) and passed through a notch filter (NF488-15, Thorlabs) to eliminate 488 nm photons. The image was then formed onto a

sCMOS sensor (PCO.edge 5.5, PCO). The 20x magnification yielded a field of view of 1 x 0.8 mm^2, with a pixel area of 0.4 x 0.4 μm^2.

Specimen chamber and visual stimulation. Both setups included a lab-built chamber filled with E3 embryo medium, and connected to the specimen holder *via* a soft membrane. This allowed us to position the larva using a combination of translation and rotation stages, while maintaining the chamber fixed with respect to the optical system. A blue LED (5 cd, 15° aperture angle), was positioned inside the chamber 6 cm in front of the fish eyes. The stimulus intensity was calibrated by measuring the radiance at a similar distance as a function of the applied voltage. In a typical experiment, we applied twenty successive 30 ms-long flashes at each intensity (3.5 ; 900 ; 1,800 ; 2,700 ; 3,600 ; 4,500 μWcm^{-2}), separated by 10 s intervals (120 flashes, 1,200 s). Image acquisition, mirror scanning, objective motion and visual stimulation were synchronized using a D/A multifunction card (NI USB-6259 NCS, National Instruments) and a custom-written program in LabVIEW (National Instruments).

Lateral and axial resolution

In light-sheet imaging, the axial and lateral resolutions are decoupled. The lateral resolution is set by the optical properties of the detection arm (detection objective and camera sensor). With our configurations, it is thus similar in both imaging methods. The axial resolution is mostly controlled by the thinness of the light sheet. In one-photon, the axial resolution, defined as the full width at half maximum (*FWHM*) of the fluorescence profile, is directly given by the light-sheet profile, which reads[1]:

$$FWHM_{1P}(x) = \sqrt{2ln(2)}\frac{\lambda_{1P}}{\pi(NA)_{1P}}\sqrt{1+\left(\frac{x}{b_{1P}}\right)^2} \quad (1)$$

where λ_{1P} is the wavelength, NA_{1P} the numerical aperture of the illumination objective, and $b_{1P}=2n\lambda_{1P}/\pi(NA)_{1P}^2$ defines the characteristic distance over which the axial resolution can be considered uniform.

In two-photon imaging, the fluorescence signal is proportional to the square of the illumination profile, such that the fluorescence profile reads:

$$FWHM_{2P}(x) = \sqrt{ln(2)}\frac{\lambda_{2P}}{\pi(NA)_{2P}}\sqrt{1+\left(\frac{x}{b_{2P}}\right)^2} \quad (2)$$

where $b_{2P}=2n\lambda_{2P}/\pi(NA)_{2P}^2$. Since $\lambda_{1P}\cong\lambda_{2P}$, it is possible to obtain the same axial resolution between the two imaging systems across the entire field of view, by setting $(NA)_{2P}=\sqrt{2}(NA)_{1P}$ through appropriate filling of the back aperture of the illumination objectives.

The fluorescence axial profile was characterized by imaging 100 nm in diameter fluorescent beads embedded in an agarose gel cylinder as they were scanned vertically across the laser sheet (**Supplementary Fig. 3a**). The recorded intensity signal of each bead exhibited a Gaussian profile from which the *FWHM* was extracted (**Supplementary Fig. 3b**). The profiles were found invariant along the scanning direction and were correctly described by equations (1) and (2) (**Supplementary Fig. 3c**). In our configuration $(NA)_{1P}=0.04$ and $(NA)_{2P}=0.055\cong\sqrt{2}(NA)_{1P}$ such that the two systems yield the same axial resolution across the field of view, as evidenced by the superposition of the measured *FWHM* profiles. If we define, as a criterium for single-cell resolution, the fact that *FWHM* is less than 6.5 µm

(the typical distance between neighboring somas), then both techniques are single-cell resolved over a band of width of 250 µm, a region that encompasses ≈80% of the brain volume.

Data pre-processing

Image processing was performed offline using Matlab (The MathWorks). We first corrected for specimen drift by registrating each image with the initial one. We implemented a semi-automatic segmentation procedure, adapted from (ref. 2), to identify individual somas and neuropil subregions (**Supplementary Fig. 4**). We then extracted the $\Delta F/F$ signal from the fluorescence trace of each ROI.

Comparative analysis of brain-wide visual response during 2P *vs* 1P imaging

In order to quantitatively compare the visually-evoked response measured using 2P and 1P light-sheet imaging, we manually selected, in each experiment (performed successively on the same fish, in approximately the same layer), five subregions that exhibited the strongest response. We then averaged the $\Delta F/F$ signal over the neurons within each region, and finally produced a post-stimulus averaged signal over the successive flash presentations, for each stimulus intensity (**Supplementary Fig. 5**). Notice that the level of spontaneous activity measured with either technique was found comparable, which indicates that 1P illumination does not impede measurement of neural activity but induces a massive reduction in visual sensitivity.

We finally run a comparative test in which the illumination intensity of the 1P light sheet was reduced down to 100 µW (as measured before the illumination objective). Even for such a low illumination power, the reduction in visual sensitivity induced by 1P imaging remains severe (**Supplementary Fig. 6**).

Cluster analysis of bright and dark flash-induced response

Optical setup. These experiments were performed on a 2P light-sheet imaging setup (**Supplementary Fig. 2**, see also ref. 10). The average laser power at λ = 930 nm was adjusted to 160 mW before the objective of a single illumination arm. Green fluorescence was detected with a laser rejection filter (FF01-680/SP, Semrock) and a green detection bandpass filter (FF01-525/50, Semrock). Images spanning 335 x 667 µm^2 of the sample with 0.67 µm pixel size, were acquired at a rate of 4.2 frames s^{-1}. We specifically designed a liquid-filled chamber to enable visual stimulation of the sample. This chamber was directly suspended to the water immersion objective lenses, and provided access to the specimen from six directions of space. The agarose cylinder embedding the larva was held from the top, and the transparent bottom of the chamber was used for visual stimulation. Visual stimuli consisted of bright (200 ms) and dark (1 s) flashes in the 600-700 nm wavelength range, generated by a video projector (Vivitek Qumi Q5) and projected onto a small screen positioned at the bottom of the microscope specimen chamber using a 1/20 magnification relay optics and covering 60° of the animal visual field. Stimulation patterns were generated at a frame rate of 60 Hz by a custom C++ program using OpenGL. Image acquisition and visual stimuli were synchronously triggered using TTL pulses.

Clustering procedure. In order to identify clusters of correlated neurons, we computed the N x N Pearson correlation matrix M, where N is the number of monitored neurons. The distribution of the elements $M_{i,j}$, *i.e.* the neuron-neuron activity correlations, displayed a systematic bias towards positive values as a result of minute fluctuations of the laser intensity. This uniform correlated noise was reflected in the existence of a large eigenvalue λ of the matrix M, associated with an eigenvector V. We corrected for this effect by subtracting $\lambda V_i V_j$ from each element $M_{i,j}$. We used the k-means

algorithm to identify clusters of correlated neurons from the corrected Pearson matrix. In this clustering method, the total number k of clusters is manually set. It defines the level of coarse graining in the description of the neural dynamics. We obtained cluster maps for arbitrary numbers of clusters (*k*=10, 27 and 137 clusters in **Supplementary Fig. 8**). We computed the clusters' neuronal activity by averaging the $\Delta F/F$ signals of the associated neurons (**Supplementary Fig. 8**). The low-dimensional representation of the network dynamics was then obtained by computing the across-trial averages of each identified cluster.

Analysis and statistical methods

All analyses were done in MATLAB (The MathWorks). Error bars in figures show the standard deviation. The comparative experiments between 2P and 1P imaging were replicated on *n*=9 larvae. We checked that the order in which the two experiments were performed had no influence on these observations. The visual/hindbrain clusters dynamics evoked by bright and dark flashes were qualitatively reproduced in *n*=3 fishes, although the exact morphology of the clusters identified by k-means may vary from run to run.

Online methods references

1. Akerboom, J. *et al.*,*J. Neurosci.***32**, 13819-13840 (2012)
2. Mahou, P., Vermot, J., Beaurepaire E. & Supatto, W., *Nat. Meth.***11**, 600-601 (2014)